PCCP

PAPER

View Article Online
View Journal | View Issue

Cite this: *Phys. Chem. Chem. Phys.*, 2014, **16**, 15381

A QM/MM MD insight into photodynamics of hypoxanthine: distinct nonadiabatic decay behaviors between keto-N7H and keto-N9H tautomers in aqueous solution†

Xugeng Guo, Yuan Zhao and Zexing Cao*

Received 5th May 2014,
Accepted 30th May 2014

DOI: 10.1039/c4cp01928h

www.rsc.org/pccp

Extensive *ab initio* surface-hopping dynamics simulations have been used to explore the excited-state nonadiabatic decay of two biologically relevant hypoxanthine keto-N7H and keto-N9H tautomers in aqueous solution. QM/MM calculations and QM/MM-based MD simulations predict different hydrogen bonding networks around these nucleobase analogues, which influence their photodynamical properties remarkably. Furthermore, different solvent effects on the conical intersection formation of keto-N7H and keto-N9H were found in excited-state MD simulations, which also change the lifetimes of the excited states. In comparison with the gas-phase situation, the $S_1 \rightarrow S_0$ nonradiative decay of keto-N7H is slightly faster, while this decay process of keto-N9H becomes much slower in water. The presence of π-electron hydrogen bonds in the solvated keto-N7H is considered to facilitate the $S_1 \rightarrow S_0$ nonradiative decay process.

1. Introduction

There is an increasing interest in characterizing the photochemistry and photophysics of electronically excited states of nucleobases.[1] As the fundamental building blocks of life, these nucleic acid bases may undergo extremely ultrafast nonradiative decay in vacuum, solution and DNA environments upon UV irradiation. It was found that the hydrogen bonding networks of the DNA bases with the surrounding environments play a crucial role in their photostability.[2]

In recent years, the photoinduced excited-state dynamics of a rare naturally occurring DNA nucleobase analogue hypoxanthine has been investigated by a range of experimental techniques, where the pump wavelengths are in the range between 255 and 270 nm, slightly longer than the experimentally measured absorption maximum of ~250 nm in aqueous solution.[3–5] Temps and co-workers comprehensively studied the ultrafast electronic deactivation dynamics of hypoxanthine and its derivatives by using femtosecond time resolved absorption and fluorescence spectroscopy, and they observed that in aqueous solution hypoxanthine returns to the electronically ground state at a time constant of 0.21 ± 0.08 ps after photoexcitation.[3] Peón and co-workers subsequently reported a similar excited-state lifetime ($\tau < 0.20$ ps) by means of a femtosecond fluorescence up-conversion experiment.[4] More recently, Chen and Kohler applied the femtosecond transient absorption spectroscopy to obtain a shorter time constant of 0.13 ± 0.02 ps, and it was viewed as a candidate with the shortest excited-state lifetime among the studied natural or modified nucleobases.[5]

In addition to current experimental studies, quantum chemical computations and dynamics simulations have been directed at understanding hypoxanthine's photophysics.[4,6–10] This compound has multiple tautomers, in which the keto-N7H and keto-N9H forms are found to be dominant with approximately equal amounts in methanol solution (53–54% for keto-N7H);[4] however, there is no accurate information on their relative population in aqueous solution. According to theoretical calculations, keto-N7H is predicted to be less than 1 kcal mol^{-1} more stable than keto-N9H in the gas phase.[9,10] Recently, Peón and co-workers carried out the multireference configuration interaction with single excitation (MR-CIS) calculations to address a readily accessible conical intersection between the bright $S_1(^1\pi\pi^*)$ singlet state and the S_0 ground state for both tautomers.[4] In our previous studies, four direct "*ethylenic*" deactivation pathways from $S_1(^1\pi\pi^*)$ to S_0 could be reached through a barrierless

State Key Laboratory for Physical Chemistry of Solid Surfaces and Fujian Provincial Key Lab of Theoretical and Computational Chemistry, College of Chemistry and Chemical Engineering, Xiamen University, Xiamen 361005, P. R. China.
E-mail: zxcao@xmu.edu.cn

† Electronic supplementary information (ESI) available: Relative energy profiles along the LIIC reaction path from the S_0 state to the conical intersection between S_0 and S_1 states of keto-N9H. The 6 optimized geometries of both tautomers from 6 sample snapshots. Distribution of the $\delta(C_2–N_3)$ and $\delta(N_1–C_2)$ bond lengths of keto-N7H and keto-N9H at the $S_1 \rightarrow S_0$ hopping points. Predicted key geometric parameters in the gas phase and aqueous solution along with the experimental crystal data. Cartesian coordinates (Å) of the QMMM-optimized representative local ground-state geometries. See DOI: 10.1039/c4cp01928h

way, and the following *ab initio* on-the-fly dynamics simulations in the gas phase lend support to this fact.[10] In addition, we also noted that the solvatochromic effects on their vertical excitation energies are quite different, with a red-shift of 0.04 eV for keto-N7H and a blue-shift of 0.06 eV for keto-N9H.[10]

Despite such important contributions, the sophisticated computational characterization of the excited-state dynamics of keto-N7H and keto-N9H in aqueous solution is still unavailable to our best knowledge, and several key questions about the nature of the solvent effect and the detailed mechanisms for nonradiative decay processes in solution remain open. For instance, (i) what are the hydrogen-bond features for both forms at different states? (ii) And what are the solvent effects on their excited-state lifetimes and deactivation behaviors? In an attempt to clarify these issues, we here perform the combined quantum mechanical/molecular mechanical molecular dynamics (QM/MM MD) simulations to explore the ultrafast nonadiabatic decay of two biologically relevant hypoxanthine keto-N7H and keto-N9H tautomers in aqueous solution. It was expected that the state-of-the-art surface-hopping dynamics simulations can improve the understanding of their intrinsic photophysical properties in solution.

2. Computational details

The geometry optimizations of keto-N7H and keto-N9H tautomers in aqueous solution were carried out using the CHEMSHELL 3.5[11] package integrating the AMBER 12[12] and TURBOMOLE 6.4[13] programs. The model was constructed by placing each tautomer in a cubic box of TIP3P[14] water molecules with length of a side being more than 24 Å. Herein, the charge and force field parameters were treated by the restrained electrostatic potential (RESP)[15] and the AMBER GAFF[16] schemes, respectively. The 10 Å cutoff was applied for the electrostatic interaction calculations. Following the energy minimization procedure, MD simulations were performed. In particular, the system was heated to 300 K, and then 1 ns equilibration was carried out along with the constant pressure periodic boundary conditions. The SHAKE[17,18] algorithm was used to constrain all of the bonds related to hydrogen atoms. The 6 sample snapshots extracted from the equilibrated configurations of each solvated base analogue by MD simulations were considered as the starting structures for the following QM/MM optimizations. Here, the QM region including keto-N7H or keto-N9H was computed at the B3LYP/def-SVP level, while the MM region was depicted by the AMBER force field. The hybrid delocalized coordinates (HDLC)[19] technique was finally employed during the geometry optimization.

The hybrid cluster-continuum model was used to calculate the vertical excitation energies of two low-lying excited singlet states, in which the small cluster model containing the base analogue and several explicit water molecules was extracted from the QM/MM optimized equilibrium configuration in aqueous solution. The polarizable continuum model (PCM) was used to explore the bulk solvent effect. In calculations of time-dependent density functional theory (TD-DFT), three functionals including B3LYP, and X3LYP and M06-2X along with an aug-cc-pVDZ basis set were employed. The TD-DFT calculations were performed using the TURBOMOLE 6.4[13] and GAUSSIAN 09[20] programs.

Photoinduced nonadiabatic dynamics was performed for the two species by the fewest switches trajectory surface-hopping method,[21] as implemented with the NEWTON-X[22,23] program integrating the COLUMBUS[24–26] and TINKER[27] packages. The *ab initio* calculations (QM region) were employed at the state-averaged complete active space self-consistent-field (SA-CASSCF) level. Here CAS was composed of ten electrons distributed into eight π-orbitals, namely, CAS(10e/8o). State-averaging over two states was considered, and a 6-31G(d) basis set was employed for all atoms. In order to approximately evaluate the CASSCF performance of the potential energy surface of the low-lying states, the relative energy profiles along the linearly interpolated internal coordinate (LIIC) reaction path from the S_0 state to the S_0/S_1 conical intersection of keto-N9H were predicted by CASSCF and CASPT2, and a reasonable agreement between both the calculations has been found (see Fig. S1 of the ESI†). The molecular mechanics (MM) region was described by the OPLS-AA force field.[28] The TIP3P model was chosen for the solvent water, and 833 molecules were included in the calculation. One hundred trajectories starting at the S_1 excited state were computed for each tautomer and the maximum simulation time is 400 fs. For keto-N7H, however, trajectories that evolved into the S_0 state and stayed there for more than 100 fs were automatically terminated. The classical equations were integrated using the Velocity-Verlet algorithm[29] with a time step of 0.5 fs. Further technical details of the dynamics simulations can be found in previous studies.[30–33]

3. Results and discussion

3.1 Ground-state structures in water

The representative QM/MM-optimized structures of solvated hypoxanthine keto-N7H and keto-N9H tautomers in their S_0 states are partially plotted in Fig. 1 and 2, respectively. The 6 optimized geometries of both tautomers from 6 sample snapshots are shown in Fig. S2 and S3 (ESI†), and the key structural parameters as well as the corresponding Cartesian coordinates can be found in Tables S1–S4 (see the ESI†), together with the available experimental crystal data[34] for a direct comparison.

We note that both keto-N7H and keto-N9H have planar structures for their S_0 states in the gas phase.[10] However, in aqueous solution, their aromatic rings are found to show a slight distortion, with the $\phi(C_6–C_5–C_4–N_9)$ dihedral angles of 178.0/178.3 and 177.9°, respectively. Structurally, the solvation leads to the elongation of the $C_2–N_3$ bond by 1.3/1.4 pm for keto-N7H and 0.7 pm for keto-N9H (*cf.* Table S1, ESI†). Such notable lengthening in keto-N7H can be attributed to the fact that the π-electron of the N_3 atom was involved in the formation of H-bonds with surrounding water molecules as shown in Fig. 1. In contrast, the $N_1–C_2$ bond was shortened by 1.5/2.2 pm for keto-N7H and 0.7 pm for keto-N9H in solution. It is obvious that the present QM/MM calculations reproduce the experimental

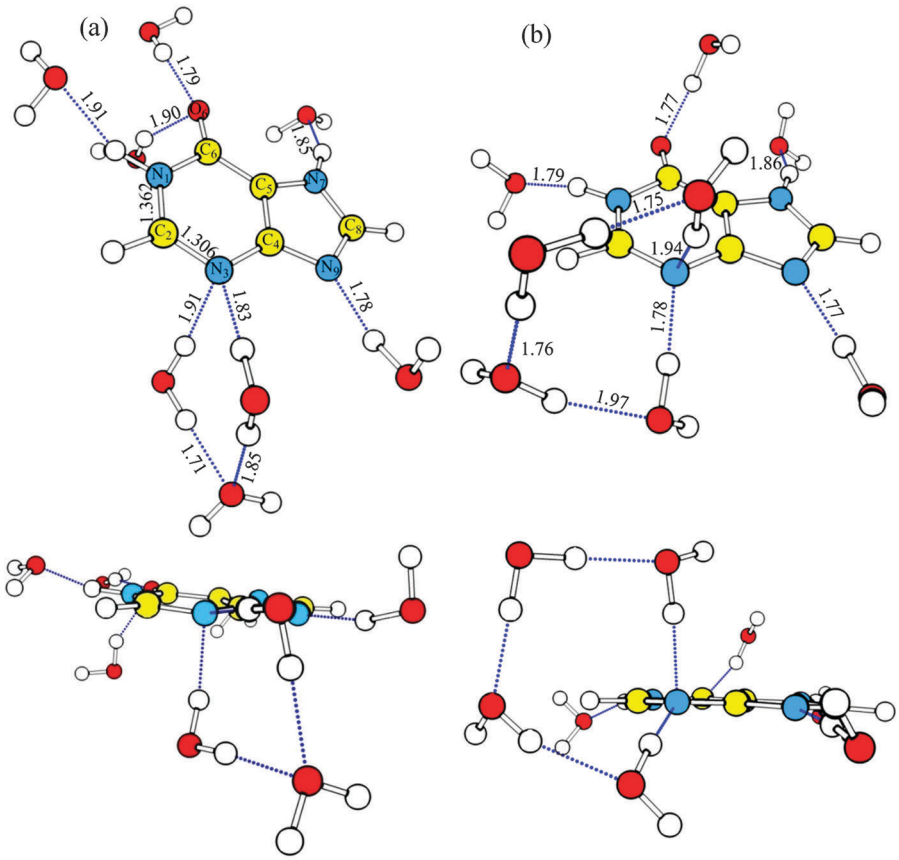

Fig. 1 QM/MM-optimized two representative local structures (a,b) and atom numbering of the hypoxanthine keto-N7H tautomer and only key hydrogen-bond interactions are shown. Upper panel: top view; lower panel: side view.

structural data reasonably (*cf.* Table S1, ESI†), and these optimized structures partially displayed in Fig. 1a and 2 can be used to generate the 100 initial configurations through the random-velocities method for the subsequent nonadiabatic dynamics simulations in aqueous solution.

As shown in Fig. 1 and 2, the H-bonding interactions around keto-N9H are slightly stronger than those around keto-N7H, and remarkable differences in the H-bonding networks around both base analogues occur at the N_3 site. In keto-N7H, there are two representative local ground-state structures from the QM/MM optimizations based on MD simulations. One structure has two relatively weak H-bonds, $\delta_1(N_3\cdots H–O)$ (1.83 Å) and $\delta_2(N_3\cdots H–O)$ (1.91 Å), and both are approximately parallel and perpendicular to the ring plane, respectively (*cf.* Fig. 1a). Similarly, the other structure has also two relatively weak H-bonds, $\delta_1'(N_3\cdots H–O)$ (1.78 Å) and $\delta_2'(N_3\cdots H–O)$ (1.94 Å), with structural similarity to $\delta_1(N_3\cdots H–O)$ and $\delta_2(N_3\cdots H–O)$, respectively (*cf.* Fig. 1b). It should be mentioned that both $\delta_2(N_3\cdots H–O)$ and $\delta_2'(N_3\cdots H–O)$ H-bonds are located below or above the ring plane, respectively. These H-bonds in keto-N7H may arise from the contribution of the lone-pair (n_N) and π electrons localized at the N_3 atom. Presumably, the presence of $\delta_2(N_3\cdots H–O)$ or $\delta_2'(N_3\cdots H–O)$ in the keto-N7H model may affect distortion of the adjacent $C_2–H_2$ bond as can be seen in the following nonadiabatic decay process (*vide infra*). For keto-N9H, a different H-bonding network was found among N_3, N_9(H) and three water molecules, with a $\delta_3(N_3\cdots H–O)$ H-bond length of 1.76 Å (*cf.* Fig. 2), which is structurally similar to $\delta_1(N_3\cdots H–O)$ of keto-N7H. This clearly indicates that both tautomers of hypoxanthine are inclined to form the different H-bonding networks in aqueous solution, and such differences in H-bonding interactions may modify their excited-state properties to a certain extent.

3.2 Vertical excitation energies

The TD-DFT-calculated vertical excitation energies of the $^1(\pi\pi^*)$ and $^1(n\pi^*)$ excited states of hypoxanthine keto-N7H and keto-N9H tautomers in the gas phase and in aqueous solution are tabulated in Table 1, together with the available experimental findings and our previous CASPT2 results.[4,10,35] It is worth mentioning that the TD-X3LYP/PCM calculations have been successfully applied to five naturally-occurring nucleic acid base systems and the maximum deviation of vertical excitation energies between theory and experiment is less than 0.2 eV.[36]

It can be seen from Table 1 that the vertical excitation energies predicted by the TD-B3LYP and TD-X3LYP methods are close to each other, while the TD-M06-2X approach overestimates the vertical excitation energies by about 0.22–0.33 eV, compared to the TD-X3LYP results. At the TD-X3LYP level of theory, the vertical excitation energies of the $^1(\pi\pi^*)$ states of

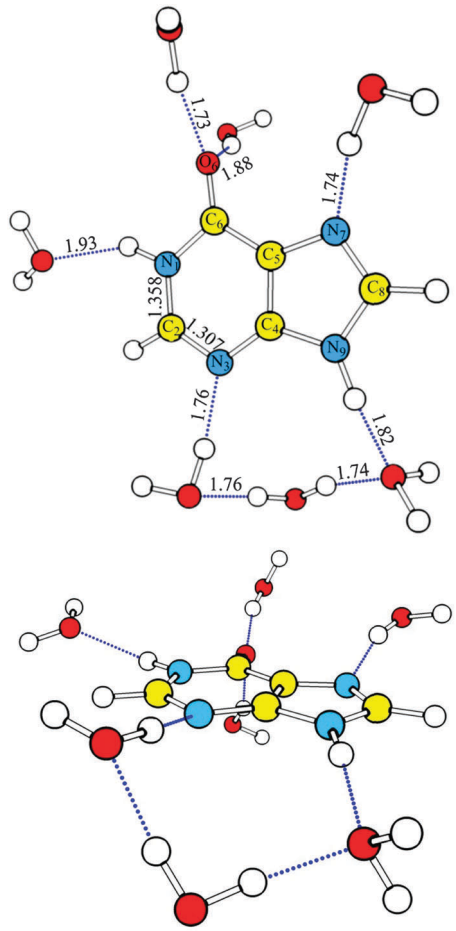

Fig. 2 QM/MM-optimized one representative structure and atom numbering of the hypoxanthine keto-N9H tautomer and only key hydrogen-bonding interactions are shown. Upper panel: top view; lower panel: side view.

keto-N7H and keto-N9H in water lie at 5.03 and 4.98 eV, respectively, showing good agreement with the available experimental value of 4.98 eV.[4] This indicates that the maximum absorption band observed in the experiment may arise from the superposition of the $^1(\pi\pi^*)$ states of the two dominant hypoxanthine tautomers, which is in accordance with the previous calculations.[4,6] On the other hand, TD-X3LYP-predicted $^1(\pi\pi^*)$ states of keto-N7H and keto-N9H in aqueous solution are blue-shifted by 0.10 and 0.24 eV, respectively, relative to the gas phase, whereas both $^1(n\pi^*)$ states exhibit the more remarkable blue shift (0.29 and 0.36 eV, respectively). We note that such a blue shift of the hypoxanthine keto-N9H tautomer is nicely consistent with that of the 9-methyl-hypoxanthine analogue (0.18 eV).[35] Considering that the relatively high $^1(n\pi^*)$ state is generally less accessible optically, it could not be expected in the subsequent nonadiabatic decay process. In the following, we will focus only on the nonadiabatic dynamics of the optically bright $^1(\pi\pi^*)$ states of keto-N7H and keto-N9H in aqueous solution (*vide infra*).

3.3 Surface hopping excited-state dynamics

Fig. 3 shows the time evolution of average occupations of the S_1 states from the respective 100 trajectories of keto-N7H and keto-N9H in aqueous solution. It can be clearly seen that after photoexcitation into the optically bright state, a faster $S_1 \rightarrow S_0$ deactivation takes place for keto-N7H.

To estimate the excited-state lifetime of keto-N7H, we have fitted its occupation of the S_1 state using a mono-exponential model within the timescale of 200 fs:

$$y = y_0 + (1 - y_0)\exp[-(t - t_1)/t_2]$$

where y_0 is the fraction of the population which does not relax to the S_0 state, t_1 is the initial delay or latency time, and t_2 is the exponential time constant. The excited-state lifetime (τ) is the sum of t_1 and t_2. The fitting process leads to $y_0 = 0$, $t_1 = 96.1$ fs, $t_2 = 16.5$ fs, and $\tau = 112.6$ fs (correlation coefficient $R^2 = 0.88$), suggesting that the dynamics of keto-N7H in aqueous solution shows a latency time of 96.1 fs before starting an ultrafast and exponential nonadiabatic decay with a decay constant of 16.5 fs. We note that the excited-state lifetime of keto-N7H in water is slightly shorter than the gas-phase result of 137.7 fs,[10] and such a similarity in two different environments shows good

Table 1 Vertical excitation energies (in eV) and oscillator strengths (in parentheses) of the $^1(\pi\pi^*)$ and $^1(n\pi^*)$ states of hypoxanthine keto-N7H and keto-N9H tautomers in vacuum and water by different theoretical approaches and experiments

		Vacuum[a]		Water[b]	
Methods	States	keto-N7H	keto-N9H	keto-N7H	keto-N9H
TD-B3LYP[c]	$^1(\pi\pi^*)$	4.90 (0.077)	4.71 (0.136)	5.12 (0.207)	5.03 (0.116)
	$^1(n\pi^*)$	5.07	5.20	5.35	5.49
TD-B3LYP[d]	$^1(\pi\pi^*)$	4.91 (0.077)	4.72 (0.136)	5.01 (0.101)	4.95 (0.150)
	$^1(n\pi^*)$	5.07	5.22	5.36	5.50
TD-X3LYP[d]	$^1(\pi\pi^*)$	4.93 (0.079)	4.74 (0.138)	5.03 (0.113)	4.98 (0.151)
	$^1(n\pi^*)$	5.12	5.18	5.41	5.54
TD-M06-2X[d]	$^1(\pi\pi^*)$	5.18 (0.101)	5.07 (0.149)	5.25 (0.206)	5.31 (0.125)
	$^1(n\pi^*)$	5.36	5.35	5.63	5.71
CASPT2[e]	$^1(\pi\pi^*)$	4.79 (0.122)	4.58 (0.167)	4.75 (0.128)	4.64 (0.175)
Expt.[f]				4.98	
Expt.[g]			4.41		4.59

[a] B3LYP/def-SVP geometry. [b] B3LYP/def-SVP/MM geometry. [c] QM (molecular + explicit water molecules)/MM. [d] QM (molecular + explicit water molecules)/PCM. [e] CCSD/6-31G(d) geometry.[10] [f] Experimental value of hypoxanthine in water at pH = 5.[4] [g] Experimental values in the vapor gas and water at pH = 6.1 from 9-methyl-hypoxanthine.[35]

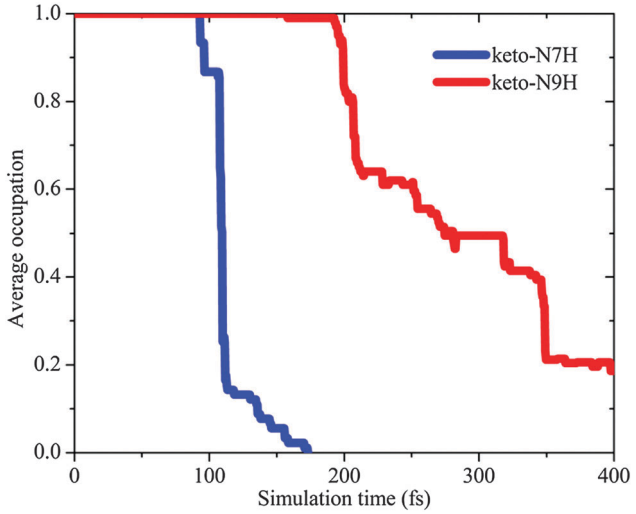

Fig. 3 Time evolution of average occupations of the S_1 states of keto-N7H and keto-N9H in aqueous solution.

agreement with the available experimental findings.[3–5] It is note worthy that the dynamics of keto-N7H in the S_1 state is not strongly affected by the steric interaction with solvent molecules.

Unfortunately, such a single exponential model cannot be applied to the fitting of the population of the S_1 state for keto-N9H. To obtain an in-depth insight into this discrepancy between photodynamical behaviors of keto-N7H and keto-N9H in water, we have, in Fig. 4, plotted both time distributions at the $S_1 \rightarrow S_0$ hopping points. We note that in the calculated 100 trajectories of keto-N7H, more than 70 ones switch to their S_0 states with time constants of approximate 110 fs, in accordance with the above estimated lifetime of 112.6 fs. However, the time distribution of keto-N9H differs from that of keto-N7H. It is basically located at two time ranges from 200 to 250 fs and from 300 to 350 fs, and thus keto-N9H exhibits a longer excited-state lifetime in aqueous solution, compared to keto-N7H, which is still close to the experimentally observed results mentioned above.[3–5] It is a reasonable assumption that keto-N7H and keto-N9H tautomers are in thermodynamic equilibrium in aqueous solution, both of which may be responsible for the ultrafast nonradiative deactivation of photoactive hypoxanthine observed in experiment.[3–5]

Quite surprisingly, the $S_1 \rightarrow S_0$ decay of keto-N9H in solution is much slower than its gas-phase counterpart with the lifetime of 85.5 fs,[10] which is different from keto-N7H and 9*H*-guanine analogues.[37] We note that the C_2–N_3 bond lengths of keto-N7H at the state-state hopping points mostly distribute below 1.4 Å, whereas those in keto-N9H generally spread above 1.4 Å, and a similar phenomenon can also be found for the N_1–C_2 bond (*cf.* Fig. S4 in the ESI†). Such structural features indicate that at the $S_1 \rightarrow S_0$ hopping points keto-N9H has much more expanding geometry than keto-N7H. Additionally, in consideration of a shorter N_1–C_2 bond of keto-N9H in water, its conical intersection structure is less accessible, compared to keto-N7H. Therefore, keto-N9H has to spend more time to evolve into the hopping point once it is promoted to the Franck–Condon region, resulting in a long excited-state lifetime.

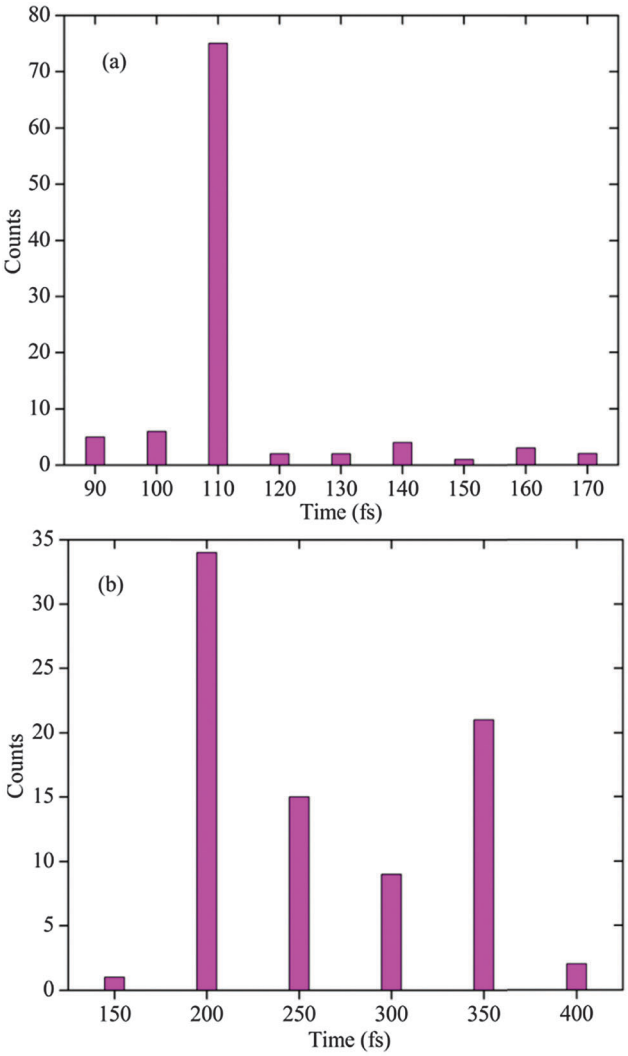

Fig. 4 Time distributions of keto-N7H (a) and keto-N9H (b) at the $S_1 \rightarrow S_0$ hopping points.

Fig. 5 shows the distributions of the $\phi(C_4$–N_3–C_2–$H_2)$ dihedral angles at the $S_1 \rightarrow S_0$ hops of keto-N7H and keto-N9H. Interestingly, each of the trajectories in keto-N7H decays to the S_0 state *via* an S_1/S_0 conical intersection with an upward distortion puckering at the C_2 atom. The ϕ-values of more than one half of the trajectories lie around -110°, partially around -90° (*cf.* Fig. 5a), which are significantly different from those in the gas phase where two slightly different kinds of conical intersections were found with approximately equal branching ratios and the corresponding ϕ-values are -82.2 and -111.5°, respectively.[10] This means that one decay channel would dominate the ultrafast nonadiabatic decay process of keto-N7H in aqueous solution. Such a behavior of keto-N7H in solution may be ascribed to the H-bonding interaction contributed by π-electrons at the N_3 site (*cf.* Fig. 1a). Presumably, the presence of such π-electron H-bonds below the ring plane may facilitate the C_2–H_2 upward out-of-plane distortion to the hopping point.

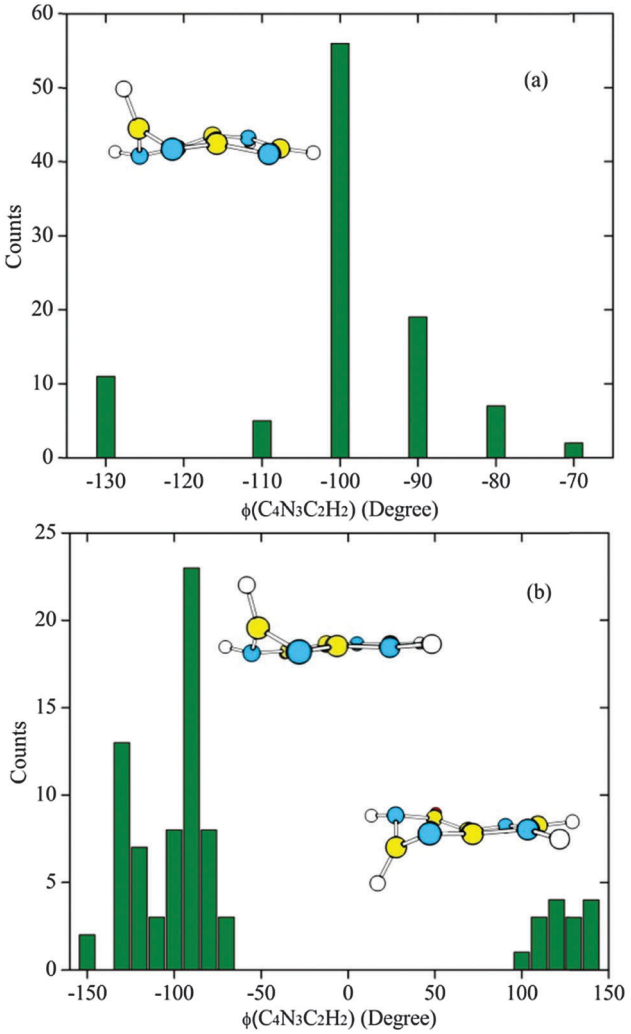

Fig. 5 Distributions of the $\phi(C_4{-}N_3{-}C_2{-}H_2)$ dihedral angles at the $S_1 \rightarrow S_0$ hops of keto-N7H (a) and keto-N9H (b). The geometries shown as insets are the representative hopping structures.

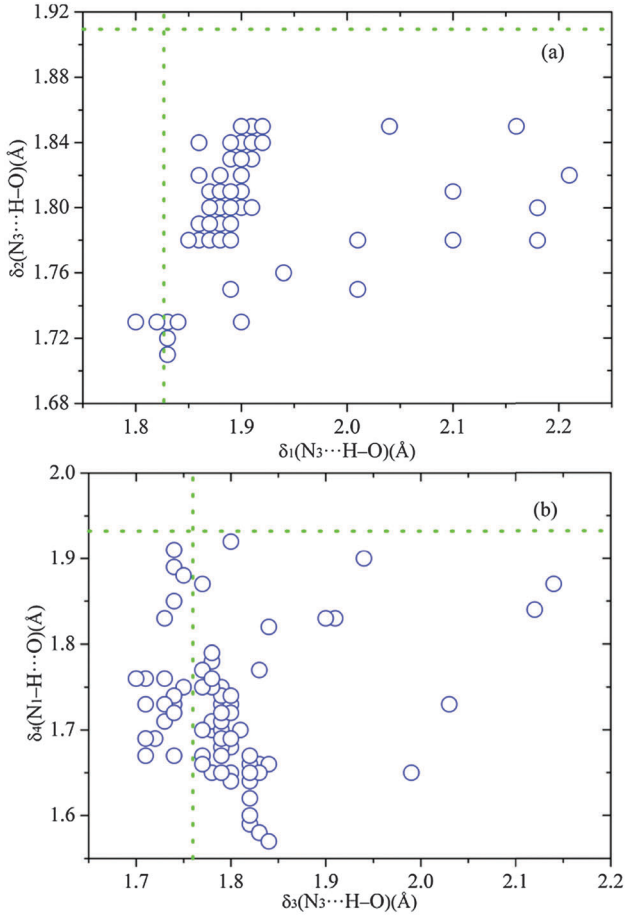

Fig. 6 Distributions of key H-bond lengths at the $S_1 \rightarrow S_0$ hopping points of keto-N7H (a) and keto-N9H (b). Green lines represent the corresponding values in their ground states: (a) 1.83 and 1.91 Å; (b) 1.76 and 1.93 Å.

This is one reason why the $S_1 \rightarrow S_0$ decay of keto-N7H in solution is slightly faster than that in vacuum.

As mentioned above, there is another representative structure with the π-electron H-bond above the ring plane of keto-N7H (*cf.* Fig. 1b). Presumably, the presence of such π-electron H-bonds of keto-N7H may promote the downward distortion puckering at the C_2 atom during evolution to the conical intersection, like its counterpart (*cf.* Fig. 1a). Accordingly, both representative solvated structures of keto-N7H shown in Fig. 1 have similar excited-state dynamical behaviors.

For keto-N9H, 82 out of 100 trajectories can relax back to the S_0 states, where the conical intersection structures of 67 show an upward deformation puckering at the C_2 atom, while 15 are predicted to have a downward distortion at the same position. The remaining 18 are trapped in the S_1 states. As displayed in Fig. 5b, their ϕ-values are mainly located at two regions between 100 and 140° and between −80 and −130°, respectively. Obviously, keto-N9H exhibits more patterns of conical intersections than keto-N7H in our present dynamics simulations, due to the absence of π-electron H-bonds.

Fig. 6 presents the distributions of four key H-bonds at the $S_1 \rightarrow S_0$ hopping points of keto-N7H and keto-N9H. It is apparent that all $S_1 \rightarrow S_0$ hops in keto-N7H lead to the shortening of $\delta_2(N_3\cdots H{-}O)$ and simultaneously the lengthening of $\delta_1(N_3\cdots H{-}O)$ H-bond lengths (*cf.* Fig. 6a). The significantly enhanced $\delta_2(N_3\cdots H{-}O)$ H-bond can promote the evolution of keto-N7H at the S_1 state to the conical intersection, with the upward distortion as mentioned above. In contrast, the $\delta_3(N_3\cdots H{-}O)$ H-bond of keto-N9H becomes much weaker at most of the S_1/S_0 hopping points (61 trajectories) than in the ground state (1.76 Å) (*cf.* Fig. 6b). Clearly, the remarkable differences in intermolecular H-bonding interactions around keto-N7H and keto-N9H account for their distinct excited-state dynamical behaviors such as excited-state lifetimes and deactivation pathways in water.

4. Conclusions

The excited-state dynamics of two most stable hypoxanthine tautomers (keto-N7H and keto-N9H) in aqueous solution has been investigated by means of the hybrid QM/MM MD

simulations. The present results suggest that the $S_1 \rightarrow S_0$ decay of keto-N7H in water is slightly faster, while the evolution of keto-N9H to the S_0 state is much slower than in vacuum. In aqueous solution, there is one dominant decay pathway for keto-N7H, but the decay channels of keto-N9H are less sensitive to the solvent effect. Such distinct photodynamical behaviors can be ascribed to the H-bonding network differences around keto-N7H and keto-N9H in the water environment. The presence of π-electron H-bonds at the N_3 site and its evolution along the conical intersection formation play an important role in the photodynamics of keto-N7H in water. The structural features of S_1/S_0 hopping configurations and their accessibilities provide a basis for understanding of their excited-state lifetimes and the possible nonradiative decay channels in aqueous solution.

Acknowledgements

This work was supported by the National Science Foundation of China (NSFC) (Grant No. 21133007 and 21373164) and the Ministry of Science and Technology (Grant No. 2011CB808504 and 2012CB214900).

References

1 C. E. Crespo-Hernández, B. Cohen, P. M. Hare and B. Kohler, *Chem. Rev.*, 2004, **104**, 1977–2019.
2 T. Zelený, M. Ruckenbauer, A. J. A. Aquino, T. Müller, F. Lankaš, T. Dršata, W. L. Hase, D. Nachtigallova and H. Lischka, *J. Am. Chem. Soc.*, 2012, **134**, 13662–13669.
3 K. Röttger, R. Siewertsen and F. Temps, *Chem. Phys. Lett.*, 2012, **536**, 140–146.
4 J. P. Villabona-Monsalve, R. Noria, S. Matsika and J. Peón, *J. Am. Chem. Soc.*, 2012, **134**, 7820–7829.
5 J. Chen and B. Kohler, *Phys. Chem. Chem. Phys.*, 2012, **14**, 10677–10689.
6 M. K. Shukla and J. Leszczynski, *Int. J. Quantum Chem.*, 2005, **105**, 387–395.
7 M. K. Shukla and J. Leszczynski, *J. Phys. Chem. A*, 2003, **107**, 5538–5543.
8 E. Mburu and S. Matsika, *J. Phys. Chem. A*, 2008, **112**, 12485–12491.
9 B. Hernández, F. J. Luque and M. Orozco, *J. Org. Chem.*, 1996, **61**, 5964–5971.
10 X. Guo, Z. Lan and Z. Cao, *Phys. Chem. Chem. Phys.*, 2013, **15**, 10777–10782.
11 P. Sherwood, A. H. de Vries, M. F. Guest, G. Schreckenbach, C. R. A. Catlow, S. A. French, A. A. Sokol, S. T. Bromley, W. Thiel, A. J. Turner, S. Billeter, F. Tersegen, S. Thiel, J. Kendrick, S. C. Rogers, J. Casci, M. Watson, F. King, E. Karlsen, M. Sjovoll, A. Fahmi, A. Schäfer and C. Lennartz, *THEOCHEM*, 2003, **632**, 1–28.
12 D. A. Case, T. A. Darden, T. E. Cheatham, C. L. Simmerling, J. Wang, R. E. Duke, R. Luo, R. C. Walker, W. Zhang, K. M. Merz, B. Roberts, S. Hayik, A. Roitberg, G. Seabra, J. Swails, A. W. Goetz, I. Kolossváry, K. F. Wong, F. Paesani, J. Vanicek, R. M. Wolf, J. Liu, X. Wu, S. R. Brozell, T. Steinbrecher, H. Gohlke, Q. Cai, X. Ye, J. Wang, M.-J. Hsieh, G. Cui, D. R. Roe, D. H. Mathews, M. G. Seetin, R. Salomom-Ferrer, C. Sagui, V. Babin, T. Luchko, S. Gusarov, A. Kovalenko and P. A. Kollman, *AMBER 12*, University of California, San Francisco, CA, 2012.
13 R. Ahlrichs, M. Bär, M. Häser, H. Horn and C. Kölmel, *Chem. Phys. Lett.*, 1989, **162**, 165–169.
14 W. L. Jorgensen, *J. Am. Chem. Soc.*, 1981, **103**, 335–340.
15 C. I. Bayly, P. Cieplak, W. D. Cornell and P. A. Kollman, *J. Phys. Chem.*, 1993, **97**, 10269–10280.
16 J. Wang, R. M. Wolf, J. W. Caldwell, P. A. Kollman and D. A. Case, *J. Comput. Chem.*, 2004, **25**, 1157–1174.
17 J.-P. Ryckaert, G. Ciccotti and H. J. C. Berendsen, *J. Comput. Phys.*, 1977, **23**, 327–341.
18 S. Miyamoto and P. A. Kollman, *J. Comput. Chem.*, 1992, **13**, 952–962.
19 S. R. Billeter, A. J. Turner and W. Thiel, *Phys. Chem. Chem. Phys.*, 2000, **2**, 2177–2186.
20 M. J. Frisch, G. W. Trucks, H. B. Schlegel, G. E. Scuseria, M. A. Robb, J. R. Cheeseman, G. Scalmani, V. Barone, B. Mennucci, G. A. Petersson, H. Nakatsuji, M. Caricato, X. Li, H. P. Hratchian, A. F. Izmaylov, J. Bloino, G. Zheng, J. L. Sonnenberg, M. Hada, M. Ehara, K. Toyota, R. Fukuda, J. Hasegawa, M. Tshida, T. Nakajima, Y. Honda, O. Kitao, H. Nakai, T. Vreven, J. A. Montgomery, J. E. Peralta, F. Ogliaro, M. Bearpark, J. J. Heyd, E. Brothers, K. N. Kudin, V. N. Staroverov, R. Kobayashi, J. Normand, K. Raghavachari, A. Rendell, J. C. Burant, S. S. Tyengar, J. Tomasi, M. Cossi, N. Rega, J. M. Millam, M. Klene, J. E. Knox, J. B. Cross, V. Bakken, C. Adamo, C. Jaramillo, J. W. Ochterski, R. L. Martin, K. Morokuma, V. G. Zakrzewski, G. A. Voth, P. Salvador, J. J. Dannenberg, S. Dapprich, A. D. Daniels, Ö. Farkas, J. B. Foresman, J. V. Ortiz, J. Cioslowski and D. J. Fox, *Gaussian 09, Revision A.02*, Gaussian Inc., Wallingford, CT, 2009.
21 J. C. Tully, *J. Chem. Phys.*, 1990, **93**, 1061–1071.
22 M. Barbatti, G. Granucci, M. Ruckenbauer, F. Plasser, J. Pittner, M. Persico and H. Lischka, *NEWTON-X: a package for Newtonian dynamics close to the crossing seam, version 1.2*, 2011.
23 M. Barbatti, G. Granucci, M. Persico, M. Ruckenbauer, M. Vazdar, M. Eckert-Maksic and H. Lischka, *J. Photochem. Photobiol., A*, 2007, **190**, 228–240.
24 H. Lischka, R. Shepard, F. B. Brown and I. Shavitt, *Int. J. Quantum Chem.*, 1981, **S15**, 91–100.
25 H. Lischka, R. Shepard, R. M. Pitzer, I. Shavitt, M. Dallos, T. Müller, P. G. Szalay, M. Seth, G. S. Kedziora, S. Yabushita and Z. Y. Zhang, *Phys. Chem. Chem. Phys.*, 2001, **3**, 664–673.
26 H. Lischka, R. Shepard, I. Shavitt, R. M. Pitzer, M. Dallos, T. Müller, P. G. Szalay, F. B. Brown, R. Ahlrichs, H. J. Boehm, A. Chang, D. C. Comeau, R. Gdanitz, H. Dachsel, C. Ehrhardt, M. Ernzerhof, P. Höchtl, S. Irle, G. Kedziora, T. Kovar, V. Parasuk, M. J. M. Pepper, P. Scharf, H. Schiffer, M. Schindler, M. Schüler, M. Seth, E. A. Stahlberg, J.-G. Zhao, S. Yabushita, Z. Zhang, M. Barbatti, S. Matsika,

M. Schuurmann, D. R. Yarkony, S. R. Brozell, E. V. Beck, J.-P. Blaudeau, M. Ruckenbauer, B. Sellner, F. Plasser and J. J. Szymczak, *COLUMBUS, an ab initio electronic structure program, release 7.0*, 2012.
27 J. W. Ponder and F. M. Richards, *J. Comput. Chem.*, 1987, **8**, 1016–1024.
28 W. L. Jorgensen and N. A. McDonald, *THEOCHEM*, 1998, **424**, 145–155.
29 W. C. Swope, H. C. Andersen, P. H. Berens and K. R. Wilson, *J. Chem. Phys.*, 1982, **76**, 637–649.
30 M. Barbatti and H. Lischka, *J. Am. Chem. Soc.*, 2008, **130**, 6831–6839.
31 M. Ruckenbauer, M. Barbatti, T. Müller and H. Lischka, *J. Phys. Chem. A*, 2010, **114**, 6757–6765.
32 M. Ruckenbauer, M. Barbatti, B. Sellner, T. Müller and H. Lischka, *J. Phys. Chem. A*, 2010, **114**, 12585–12590.
33 M. Ruckenbauer, M. Barbatti, T. Müller and H. Lischka, *J. Phys. Chem. A*, 2013, **117**, 2790–2799.
34 H. W. Schmalle, G. Hänggi and E. Dubler, *Acta Crystallogr., Sect. C: Cryst. Struct. Commun.*, 1988, **44**, 732–736.
35 L. B. Clark and I. Tinoco, *J. Am. Chem. Soc.*, 1965, **87**, 11–15.
36 Y. Zhao and Z. Cao, *J. Theor. Comput. Chem.*, 2013, **12**, 1341013.
37 B. Heggen, Z. Lan and W. Thiel, *Phys. Chem. Chem. Phys.*, 2012, **14**, 8137–8146.

